

Impacts of Heat Flux Distribution, Sloping Magnetic Field and Magnetic Nanoparticles on the Natural Convective Flow Contained in a Square Cavity

Latifa M. Al-Balushi and M. M. Rahman*

Department of Mathematics, College of Science, Sultan Qaboos University, Muscat, Oman

*Corresponding Author: M. M. Rahman. Email: mansurdu@yahoo.com

Received: 06 September 2019; Accepted: 11 December 2019

Abstract: In the present paper, the effect of the heat flux distribution on the natural convective flow inside a square cavity in the presence of a sloping magnetic field and magnetic nanoparticles is explored numerically. The nondimensional governing equations are solved in the framework of a finite element method implemented using the Galerkin approach. The role played by numerous model parameters in influencing the emerging thermal and concentration fields is examined; among them are: the location of the heat source and its length H^* , the magnitude of the thermal Rayleigh number, the nanoparticles shape and volume fraction, and the Hartmann number. It is found that the nanofluid velocity becomes higher when the thermal source length, the nanoparticles volume fraction and/or the thermal Rayleigh number are increased, while it decreases as the Hartmann number Ha grows and the position of the heat source moves toward the center of the lower wall of the cavity. Moreover, the temperature of the nanofluid grows with the extension of the thermal source and decreases slowly when the heat flux position moves toward the center of the lower wall. The outcomes of the research also indicate that the average Nusselt number becomes smaller on increasing Hartmann number Ha and heat source length H^* . The addition of Fe_3O_4 to engine oil leads to a higher rate of heat transfer with respect to the addition of SiO_2 particles. Blade-shaped nanoparticles generate the highest value of the Nusselt number compared to all the other considered shapes.

Keywords: Nanofluids; magnetic nanoparticles; heat source; natural convection; finite element method; square enclosure

Nomenclature

B_0	magnetic field strength (NmA^{-1})
C	concentration of nanofluid ($mol\ m^{-3}$)
C_c	reference concentration ($mol\ m^{-3}$)
c_p	specific heat ($Jkg^{-1}K^{-1}$)
D_B	Brownian diffusion coefficient (m^2s^{-1})
d_p	diameter of nanoparticle (nm)
D_T	thermal diffusion coefficient (m^2s^{-1})
D	heat flux location (m)



This work is licensed under a Creative Commons Attribution 4.0 International License, which permits unrestricted use, distribution, and reproduction in any medium, provided the original work is properly cited.

D^*	dimensionless heat flux location
f	dimensionless oscillation frequency
g	acceleration due to gravity (m^2s^{-1})
k_B	Boltzmann constant (JK^{-1})
h^*	convective heat transfer coefficient
Ha	Hartmann number
H	heat flux length (m)
H^*	dimensionless heat flux length
L	length of the bottom wall (m)
Le	Lewis number
m	mass (kg)
Nu	Nusselt number
Nu_{ave}	average Nusselt number
N_{TBTC}	dynamic diffusion parameter
N_{TBT}	dynamic thermo-diffusion parameter
n	empirical shape factor of nanoparticles
p	dimensional pressure (Pa)
P	dimensionless pressure
Pr	Prandtl number
q''	heat flux (Wm^{-2})
Nb	Brownian diffusion parameter
Nt	thermophoresis parameter
Ra_T	local thermal Rayleigh number
Ra_C	local solutal Rayleigh number
Sc	Schmidt number
t	dimensional time (s)
T	temperature (K)
T_h	temperature of the hot wall (K)
T_c	temperature of the cold wall (K)
(u, v)	dimensional velocity components (ms^{-1})
(U, V)	dimensionless velocity components
(x, y)	dimensional coordinates (m)
(X, Y)	dimensionless coordinates

Greek symbols

α	thermal diffusivity (m^2s^{-1})
α_{nf}	thermal diffusivity of nanofluid (m^2s^{-1})
β	coefficient of volume expansion (K^{-1})
β^*	coefficient of mass expansion ($\text{mol}^{-1}\text{m}^3$)
γ	magnetic field sloping angle ($^\circ$)
τ	nondimensional time
ρ	fluid density (kgm^{-3})
ρ_{nf}	density of the nanofluid (kgm^{-3})
ρ_{bf}	density of the base fluid (kgm^{-3})
ρ_p	density of the solid particles (kgm^{-3})
μ	dynamic viscosity (Pas)
μ_{nf}	viscosity of the nanofluid (Pas)
μ_{bf}	viscosity of the base fluid (Pas)

ν	kinematic coefficient of viscosity
θ	dimensionless temperature
ϕ^*	nanoparticles volume fraction
Φ	dimensionless concentration
κ	thermal conductivity ($\text{Wm}^{-1}\text{K}^{-1}$)
κ_{nf}	thermal conductivity of nanofluid ($\text{Wm}^{-1}\text{K}^{-1}$)
κ_{bf}	thermal conductivity of base fluid ($\text{Wm}^{-1}\text{K}^{-1}$)
κ_p	thermal conductivity of solid particles ($\text{Wm}^{-1}\text{K}^{-1}$)
ψ	stream function
Ψ	sphericity of the nanoparticles
σ	electric conductivity (Sm^{-1})
ΔC	concentration drop (molm^{-3})
ΔT	temperature drop (K)

Subscripts

nf	nanofluid
bf	base fluid
p	solid particles
h	hot wall
c	cold wall
ave	average

1 Introduction

In most of the industrial applications upsurge in heat transfer is demanded. One of the vital mechanisms enhancing heat transfer is natural convection utilizing nanofluids which are a notable subject to most recent research papers as a result of the developing need of engineering and nanotechnology applications. Nanometer-sized particles are added to regular fluids to produce nanofluids Choi [1]. Many industrial and mechanical applications have used nanofluids due to their significant advantages in augmenting heat transfer with less clogging and reduced pumping power. Types of geometry play a significant role in the augmentation of heat transfer in nanofluids. Every cavity has its characteristics that improve the heat transfer rate. To determine the influences of heat flux on the heat transfer improvement in unsteady buoyancy-driven flow inside a square cavity filled with nanofluid, a study was conducted by Nguyen et al. [2]. They found that the thermal transport properties of nanofluid significantly affect the cooling performance of a system and the rate of heat transfer declines at higher local thermal Rayleigh number. A mixed convection flow, with heat flux fixed at the bottom wall using nanofluids in a square enclosure, was simulated numerically by Mansour et al. [3]. They observed that an increase of the heat flux length, leads to a decrease in the Nusselt number whereas an increase of the nanoparticle concentration intensifies the rate of heat transfer. Oztop et al. [4] worked computationally to investigate the mixed convection hydromagnetic flow of nanofluids inside a partially heated lid-driven cavity. They claimed that the heat transfer rate decreases when the Hartmann number strengthens. They also noticed that the increase in nanoparticle concentration enhances the Nusselt number. Recently, Esfe et al. [5] conducted a numerical experiment to study the mixed convective flow in a lid-driven enclosure occupied by various nanofluids. They noticed that Richardson and Rayleigh's numbers are two important parameters enhancing the heat transfer rate. They also showed that the geometry inclination angle has extreme effects on the total entropy generation as well as on the heat transfer rate. Moreover, they found that mixing nanoparticles to the regular fluids, decreases the entropy generation and augments the heat transfer rate. Furthermore, Bondarenko et al. [6] investigated convective phenomena to determine the rate of heat

transfer between two-adherent porous blocks in a lid-driven enclosure utilizing nanofluids. Their outcomes showed that a higher size of a porous block intensifies the Nusselt number. Astanina et al. [7] carried out the MHD free convection flow of nanofluids in a square cavity whose walls are partially heated under an externally applied magnetic field. Their outcomes exhibited that heat transfer rate inversely varied with the nanoparticle concentration, the strength of the applied magnetic field and the position of the heater. Free convection phenomena in a square cavity along with a circular cylinder whose side walls are adiabatic and the bottom wall temperature is variable, were investigated by Park et al. [8]. They noticed that isotherms are powerfully influenced by the temperature change of the bottom wall. Jahanbakhshi et al. [9] considered the effect of an external magnetic field and investigated the free convection flow of non-Newtonian fluid inside an L-shape enclosure. They found that Nusselt numbers are inversely related to the shear-thinning fluids and directly correlated with the shear-thickening fluids. Sheremet et al. [10] numerically simulated the free convection flow inside an inclined square cavity taking into consideration the time-sinusoidal variation of temperature. Their results showed that a growing oscillating frequency of the boundary tends to intensify the oscillation amplitude of the Nusselt number. Cho et al. [11] studied buoyancy-driven phenomena in a square cavity using an array of perpendicular circular and elliptical cylinders. They found that the solution reaches an unsteady state except for the value of the aspect ratio $AR = 2$ and $AR = 4$ for both lower and upper elliptical cylinders. In recent years, the rate of heat transfer for the buoyancy-driven flow is considered to be heavily and affected by the nanoparticle's shape, uniform sinusoidal roughness elements and nanoparticle random motion [12,13]. Mehryan et al. [14] studied the convection mechanism in a square enclosure occupied by solid, porous and free fluid layers. The outcomes of the study showed that the rate of heat transfer increases with the increase of the buoyancy ratio parameter Nr as well as with the increase of the Lewis number Le . Similarly, the numerical investigation for buoyancy-driven mechanism and total entropy generation in a square enclosure filled with nanofluids, using various distributions of temperature fields along with a concentric solid, was conducted by Alsabery et al. [15]. Their study showed that the inner solid size and thermal conductivity ratio respectively, control the heat transfer rate. Alsabery et al. [16] further studied numerically the buoyancy-driven flow in the presence of a corner heater and conducting block using a non-homogenous model in a square enclosure filled with nanofluids. They showed that an increase in the number of similar size blocks having the same thermal conductivity effectively intensify the Nusselt number. Sezai et al. [17] performed numerical investigation for buoyancy-driven flow induced by a discrete heat flux which was located at the bottom of a rectangular cavity. They displayed that the maximum of the Rayleigh number falls, as the heat source aspect ratio is increased. Free convection, with heat source fixed at the bottom wall of the cavity utilizing nanofluids, was examined by Aminossadati et al. [18]. They claimed that heater length and its location, vastly affect the heat transfer rate.

Saravanan et al. [19] studied numerically the buoyancy convection with two mutually orthogonal heat-generating baffles in a closed square cavity. Their investigation showed that the length of any of the baffles, which was mounted inside the cavity, directly affected the rate of heat transfer whereas there is no effect for changing the positions of the baffles. Numerical computation for natural convection in a square cavity due to two mutually orthogonal isothermal baffles and the effect of the baffles sizes and positions inside the cavity was conducted by Kandaswamy et al. [20]. Their outcomes showed that the vertical baffle length regardless of its position enhanced the rate of heat transfer. Saravanan et al. [21] investigated numerically the buoyancy-driven flow due to two mutually perpendicular heated thin plates with deferent boundary conditions in a square cavity. They found that the rate of heat transfer intensifies when one plate placed far away from the center of the cavity for isothermal boundary condition. Furthermore, buoyancy induced convection with discretely heat-generating baffles in a square cavity was examined numerically by Hakeem et al. [22]. They claimed that when the vertical baffle was located very close to the sidewall or the horizontal baffle was located very close to the bottom wall, the average Nusselt number reached its maximum.

Due to the potential applications of nanofluid in different fields of science and engineering such as solar energy, chemical, microchannel, bioengineering and automotive, it has received considerable attention by many researchers like Alsabery et al. [23,24], Al Kalbani et al. [25], Uddin et al. [26–28], Astanina et al. [29], Sathiyamoorthy et al. [30], Mehryan et al. [31] and Rahman et al. [32] who have studied the dynamics of nanofluids in various cavities. Mathematical modelling of nanofluids provides a representation of the parameters governing the problem that can be examined with the least possible cost, and thereby provide a good understanding of the situation. This can then be followed by experiments on the points of major interest. So far, the models that have been developed for nanofluids are one component model (Tiwari et al. [33]), two-component model (Buongiorno [34]) and nonhomogeneous dynamics model (Uddin et al. [35]) have been developed. Al-Balushi et al. [36] researched to investigate the free convection flow and heat transfer utilizing magnetic nanoparticles inside a square enclosure with a non-homogeneous dynamic model. They have explored the influences of the local thermal Rayleigh number, nanoparticles shape and nanoparticles concentration on the streamlines, isotherms, isoconcentrations, and the rate of heat transfer. Recently, Al-Balushi et al. [37] extended their previous work [36] taken into account the effects of an applied magnetic field and four different thermal boundary conditions which are uniform, parabolic in space, sinusoidal in space, and sinusoidal in time. They have also considered 12 different types of magnetic nanofluids. But both of their studies neglect the effects of heat flux on the flow and thermal fields. To the best of the authors' knowledge, no research has been carried out to investigate the free convection flow inside a square enclosure having constant heat flux at the bottom wall, using magnetic nanoparticles and sloping magnetic field, following non-homogeneous dynamic model.

Therefore, this study aims to extend the work of Al-Balushi et al. [37] to study the natural convection flow of magnetic nanofluids considering heat flux, having variable length and position at the bottom wall of the square cavity, applying inclined magnetic field using nonhomogeneous dynamic model. In any real life engineering applications, the geometry is more complicated than an enclosure. However, the important insights of heat transfer of a very complex design can be provided by the simple geometry. The results of this study can be helpful in analyzing heat transfer in industrial applications such as heat exchangers, solar thermal collectors and cooling of electronic equipment.

2 Formulation of the Problem

2.1 Physical Model

Let us consider the two-dimensional free convection flow of nanofluids which is unsteady, laminar and incompressible, energized by a heat flux having length H inside a square cavity of length L . The flow and thermal fields are enforced by a uniform magnetic field $\mathbf{B} = B_x i + B_y j$ of strength $B_0 = \sqrt{B_x^2 + B_y^2}$ making an angle (γ) to the positive x -axis. Fig. 1 shows the coordinates system and the geometry of the problem. Every mathematical model is based on some assumptions. The assumptions of our model are as follows:

- The heat flux $q'' = -\kappa_{nf} T_y$ is embedded within the middle part of the lower wall of the cavity whereas the upper wall is reserved at low temperature $T = T_C$.
- Two vertical walls and the remaining part of the lower wall are kept insulated.
- Thermophoresis, Brownian diffusion, and gravity effects are taken into account.
- There are no chemical reactions and negligible thermal radiation within the flow domain.
- Four types of solid spherical magnetic nanoparticles such as ferrite (Fe_3O_4), Mn-Zn ferrite ($\text{Mn-ZnFe}_2\text{O}_4$), cobalt ferrite (CoFe_2O_4) and silicon dioxide (SiO_2) and three kinds of base fluids such as water (H_2O), kerosene (Ke) and engine oil (EO) are considered.
- Nanoparticles and base fluids are supposed to remain in thermal equilibrium.

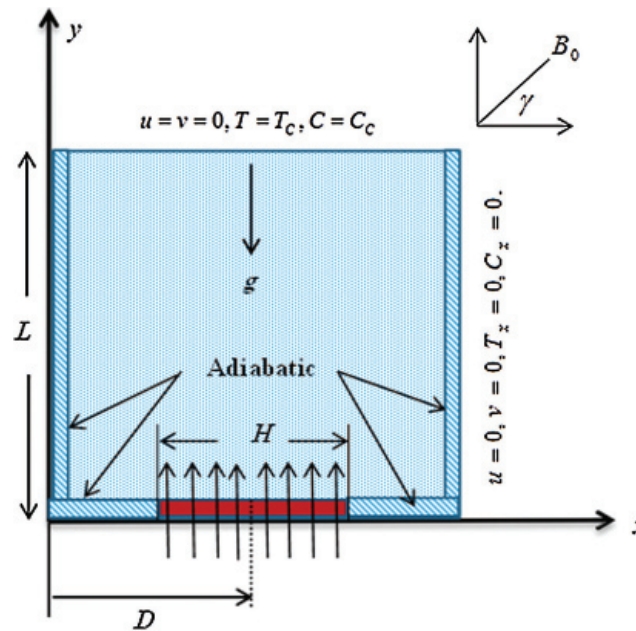


Figure 1: Physical model and coordinates system

2.2 Mathematical Modeling

2.2.1 Conservation Equation for Nanofluids

The governing continuity, momentum, energy and concentration equations are as follows (see Uddin et al. [35], Al-Balushi et al. [36,37]):

$$u_x + v_y = 0 \quad (1)$$

$$\begin{aligned} \rho_{nf} [u_t + uu_x + vv_y] = & -p_x + \mu_{nf} (u_{xx} + v_{yy}) \\ & + \sigma_{nf} B_0^2 (v \sin(\gamma) \cos(\gamma) - u \sin^2(\gamma)) \end{aligned} \quad (2)$$

$$\begin{aligned} \rho_{nf} [v_t + uv_x + vv_y] = & -p_y + \mu_{nf} (v_{xx} + v_{yy}) + (\rho\beta)_{nf} g (T - T_c) \\ & + (\rho\beta^*)_{nf} g (C - C_c) + \sigma_{nf} B_0^2 (u \sin(\gamma) \cos(\gamma) - v \cos^2(\gamma)) \end{aligned} \quad (3)$$

$$\begin{aligned} (\rho c_p)_{nf} [T_t + uT_x + vT_y] = & k_{nf} (T_{xx} + T_{yy}) \\ & + (\rho c_p)_{nf} \left[\frac{D_B}{C} (C_x T_x + C_y T_y) \right] + (\rho c_p)_{nf} \frac{D_T}{T} [(T_x)^2 + (T_y)^2] \end{aligned} \quad (4)$$

$$\begin{aligned} C_t + uC_x + vC_y = & D_B (C_{xx} + C_{yy}) \\ & + \frac{CD_T}{T} (T_{xx} + T_{yy}) + \frac{D_T}{T} [C_x T_x + C_y T_y] \end{aligned} \quad (5)$$

where the density, effective viscosity, thermal diffusivity, volumetric thermal expansion, volumetric mass expansion, heat capacitance, thermal conductivity, electric conductivity of nanofluid are defined as follows (see Uddin et al. [35]):

$$\rho_{nf} = (1 - \phi^*)\rho_{bf} + \phi^*\rho_p \quad (6)$$

$$\mu_{nf} = \mu_{bf}(1 - \phi^*)^{-2.5} \quad (7)$$

$$\alpha_{nf} = k_{nf}/(\rho C_p)_{nf} \quad (8)$$

$$(\rho\beta)_{nf} = (1 - \phi^*)(\rho\beta)_{bf} + \phi^*(\rho\beta)_p \quad (9)$$

$$(\rho\beta^*)_{nf} = (1 - \phi^*)(\rho\beta^*)_{bf} + \phi^*(\rho\beta^*)_p \quad (10)$$

$$(\rho C_p)_{nf} = (1 - \phi^*)(\rho C_p)_{bf} + \phi^*(\rho C_p)_p \quad (11)$$

$$k_{nf} = \left[\frac{k_p + (n-1)k_{bf} - (n-1)\phi^*(k_{bf} - k_p)}{k_p + (n-1)k_{bf} + \phi^*(k_{bf} - k_p)} \right] k_{bf} + \frac{(\rho c_p)_p \phi^*}{2D_T^l} \sqrt{\frac{2D_T \kappa_B T_c}{3\pi\mu_{nf}d_p}} \quad (12)$$

$$D_T = 0.126 \frac{\kappa_{nf} \lambda \beta_{bf} \mu_{nf}}{\kappa_{bf} \rho_{nf}} \quad (13)$$

$$D_B = \frac{2\kappa_B T_C}{3\pi\mu_{nf}d_p} \quad (14)$$

$$\sigma_{nf} = \frac{\sigma_p + 2\sigma_{bf} - 2\phi^*(\sigma_{bf} - \sigma_p)}{\sigma_p + 2\sigma_{bf} + \phi^*(\sigma_{bf} - \sigma_p)} \sigma_{bf} \quad (15)$$

The nanoparticle shape factor n is known by $n = 3/\Psi$, where Ψ is the sphericity, d_p is the diameter of nanoparticle, $D_T^l = \sqrt{D_T}$ is the numerical value of D_T and κ_B is the Boltzmann constant. In the right hand side in Eq. (12), additional term comes from the random motion of nanoparticles.

2.2.2 Initial and Boundary Conditions

The initial and the boundary conditions for the current problem are as follows:

For $t = 0$; entire domain

$$u = 0, v = 0, T = T_c, C = C_c, p = 0 \quad (16)$$

For $t > 0$;

$$\text{At the top wall } (0 \leq x \leq L, y = L) : u = 0, v = 0, T = T_c, C = C_c \quad (17)$$

$$\text{At the left wall } (x = 0, 0 \leq y \leq L) : u = 0, v = 0, T_x = 0, C_x = 0 \quad (18)$$

$$\text{At the right wall } (x = L, 0 \leq y \leq L) : u = 0, v = 0, T_x = 0, C_x = 0 \quad (19)$$

$$\text{At the bottom wall : } y = 0 \quad (20)$$

$$0 \leq x < (D - 0.5H) : u = v = 0, T_y = 0, C_y = 0 \quad (20a)$$

$$(D - 0.5H) \leq x \leq (D + 0.5H) : u = v = 0, T_y = -q''/\kappa_{nf}, C = C_h \quad (20b)$$

$$(D + 0.5H) \leq x \leq L : u = v = 0, T_y = 0, C_y = 0 \quad (20c)$$

2.2.3 Non-Dimensional Governing Equations

We introduce the following transformations to make Eqs. (1–5) and (16–20) dimensionless:

$$\left. \begin{aligned} U &= uL/\alpha_{bf}, \quad V = vL/\alpha_{bf}, \quad X = x/L, \quad Y = y/L, \quad H^* = H/L, \\ D^* &= D/L, \quad P = pL^2/(\rho_{bf}\alpha_{bf})^2, \quad \tau = \alpha_{bf}t/L^2, \\ \theta &= T - T_c/\Delta T, \quad \Phi = C - C_c/\Delta C \end{aligned} \right\} \quad (21)$$

where $\Delta T = q''L/\kappa_{bf}$ and $\Delta C = C_h - C_c$ are the temperature difference and the nominal concentration difference within the nanofluid, respectively. Using non-dimensional variables (21) and assuming $(\Delta C/C_c) \ll 1$ and $(\Delta T/T_c) \ll 1$; the Eqs. (1–5) are modified in non-dimensional forms as follows:

$$U_X + V_Y = 0 \quad (22)$$

$$\begin{aligned} U_\tau + UU_X + VU_Y &= -\frac{\rho_{bf}}{\rho_{nf}}P_X + \frac{\rho_{bf}\mu_{nf}}{\rho_{nf}\mu_{bf}}\text{Pr}(U_{XX} + U_{YY}) \\ &+ \frac{\sigma_{nf}}{\sigma_{bf}}\text{Pr}Ha^2[V\sin(\gamma)\cos(\gamma) - U\sin^2(\gamma)] \end{aligned} \quad (23)$$

$$\begin{aligned} V_\tau + UV_X + VV_Y &= -\frac{\rho_{bf}}{\rho_{nf}}\frac{\partial P}{\partial Y} + \frac{\rho_{bf}\mu_{nf}}{\rho_{nf}\mu_{bf}}\text{Pr}(V_{XX} + V_{YY}) \\ &+ \frac{\rho_{bf}(\rho\beta)_{nf}}{\rho_{nf}\beta_{bf}\rho_{bf}}Ra_T\text{Pr}\theta + \frac{\rho_{bf}}{\rho_{nf}}Ra_C\text{Pr}\Phi + \frac{\sigma_{nf}}{\sigma_{bf}}\text{Pr}Ha^2[U\sin(\gamma)\cos(\gamma) - V\cos^2(\gamma)] \end{aligned} \quad (24)$$

$$\theta_\tau + U\theta_X + V\theta_Y = \frac{\alpha_{nf}}{\alpha_{bf}}(\theta_{XX} + \theta_{YY}) + \frac{1}{Le}(\Phi_X\theta_X + \Phi_Y\theta_Y) + \frac{\text{Pr}N_{TBT}}{Sc}[(\theta_X)^2 + (\theta_Y)^2] \quad (25)$$

$$\Phi_\tau + U\Phi_X + V\Phi_Y = \frac{\text{Pr}}{Sc}(\Phi_{XX} + \Phi_{YY}) + \frac{\text{Pr}}{Sc}[N_{TBTC}(\theta_{XX} + \theta_{YY}) + N_{TBT}(\Phi_X\theta_X + \Phi_Y\theta_Y)] \quad (26)$$

The non-dimensional parameters appeared in Eqs. (22–26) are as follows:

$\text{Pr} = \frac{\nu_{bf}}{\alpha_{bf}}$ is the Prandtl number, $Le = \frac{\kappa_{bf}C_C}{(\rho c_p)_{bf}D_B\Delta C}$ is the modified Lewis number, $Ra_T = \frac{L^3\beta_{bf}g\Delta T}{\nu_{bf}\alpha_{bf}}$ is

the local thermal Rayleigh number, $Ra_C = \frac{L^3g\Delta C(\rho\beta^*)_{nf}}{\nu_{bf}\alpha_{bf}\rho_{nf}}$ is the local solutal Rayleigh number,

$N_{TBT} = \frac{D_T\Delta T}{D_B T_C}$ is the dynamic thermo-diffusion parameter, $Sc = \frac{\mu_{bf}}{\rho_{bf}D_B}$ is the Schmidt number,

$Ha = B_0L\sqrt{\frac{\sigma_{bf}}{\rho_{bf}\nu_{bf}}}$ is the Hartmann number and $N_{TBTC} = \frac{D_T C_C \Delta T}{D_B T_C \Delta C}$ is the dynamic diffusion parameter.

2.2.4 Non-Dimensional Boundary Conditions

The non-dimensional boundary conditions (17–20) can be expressed as:

For $\tau = 0$; in the entire domain

$$U = 0, V = 0, \theta = 0, \Phi = 0, P = 0 \quad (27)$$

For $\tau > 0$:

$$\text{At the top wall } (0 \leq X \leq 1, Y = 1) : U = 0, V = 0, \theta = 0, \Phi = 0 \quad (28)$$

$$\text{At the left wall } (X = 0, 0 \leq Y \leq 1) : U = 0, V = 0, \theta_X = 0, \Phi_X = 0 \quad (29)$$

$$\text{At the right wall } (X = 1, 0 \leq Y \leq 1) : U = 0, V = 0, \theta_X = 0, \Phi_X = 0 \quad (30)$$

$$\text{At the bottom wall : } Y = 0 \quad (31)$$

$$0 \leq X < (D^* - 0.5H^*) : U = V = 0, \theta_Y = 0, \Phi_Y = 0 \quad (31a)$$

$$(D^* - 0.5H^*) \leq X \leq (D^* + 0.5H^*) : U = V = 0, \theta_Y = -\kappa_{bf}/\kappa_{nf}, \Phi = 1 \quad (31b)$$

$$(D^* + 0.5H^*) \leq X \leq 1 : U = V = 0, \theta_Y = 0, \Phi_Y = 0 \quad (31c)$$

3 Thermophysical Properties

The properties of base fluids and nanoparticles built the nanofluid's thermophysical properties. For the present investigation, the magnitudes of density, viscosity, thermal conductivity, specific heat capacity, and volumetric thermal expansion coefficients have been considered. Tab. 1 (see Uddin et al. [38]) and Tab. 2 (Hafezisefat et al. [39], Khan et al. [40] and Al-Balushi et al. [37]) represent the thermophysical properties of base fluids and solid nanoparticles respectively.

Table 1: Thermo-physical properties of the base fluids (Uddin et al. [38])

Thermo-physical properties	H ₂ O	EO	Ke
$\rho(\text{kgm}^{-3})$	997.1	888.23	780
$\mu(\text{Nsm}^{-2})$	0.001003	0.845	0.0016
$\kappa(\text{Wm}^{-1}\text{K}^{-1})$	0.613	0.145	0.149
$C_p(\text{Jkg}^{-1}\text{K}^{-1})$	4179	1880.3	2090
$\beta(\text{K}^{-1})$	21×10^{-5}	70×10^{-5}	99×10^{-5}
$\alpha \times 10^{-7}(\text{m}^2\text{s}^{-1})$	1.47	0.868	0.914
Pr	6.8377	10959	23.004

4 The Average Nusselt Number

The significant quantity for the numerical simulation is the average Nusselt number (Nu_{ave}) along the heated bottom wall. The ratio of convective to conductive heat transfer across the boundary is well-defined by the Nusselt number as follows:

Table 2: Thermo-physical properties of the solid nanoparticles (Hafezisefat et al. [39], Khan et al. [40] and Al-Balushi et al. [37])

Thermo-physical properties	Fe ₃ O ₄	CoFe ₂ O ₄	Mn-ZnFe ₂ O ₄	SiO ₂
$\rho(\text{kgm}^{-3})$	5180	4907	4900	2200
$\kappa(\text{Wm}^{-1}\text{K}^{-1})$	80.4	3.7	5	36
$C_p(\text{Jkg}^{-1}\text{K}^{-1})$	670	700	800	765
$\beta(\text{K}^{-1})$	20.6×10^{-5}	12.9×10^{-6}	1.2×10^{-6}	5.6×10^{-7}

$$Nu_s = h^*L/\kappa_{bf} \quad (32)$$

where h^* is coefficient of the convective heat transfer of the nanofluid and can be expressed by

$$h = q''/(T_s - T_c) \quad (33)$$

Using non-dimensional variables defined in (21) we have

$$Nu_s = q''L/((T_s - T_c)\kappa_{bf}) \quad (34)$$

The local Nusselt number for nanofluid for the present investigations is calculated as

$$Nu_s(X) = 1/\theta_s(X) \quad (35)$$

At the bottom heated wall, the average Nusselt number can be expressed as

$$Nu_{ave} = \frac{1}{H^*} \int_{D^*-H^*/2}^{D^*+H^*/2} (1/\theta_s(X))dX \quad (36)$$

5 Computational Procedures

Using Galerkin weighted residual brand of finite element method (FEM), the dimensionless governing Eqs. (22–26) with the boundary conditions (27–31) are simulated numerically. Well description of this method can be found in the books and papers by Uddin et al. [28], Zienkiewicz et al. [41], Zienkiewicz et al. [42], Codina [43], Uddin [44], Rahman et al. [45] and Al Kalbani et al. [46]. Thus, the explanations of this method are absent here for shortness. The numerical simulation is carried out by a PDE solver named COMSOL Multiphysics with MATLAB interface.

In FEM, we need to generate proper meshes or grids to solve the boundary value problems effectively. On the generated networks, the physical variables such as velocity, temperature and pressure are determined. In Fig. 2, we have created the meshes of the current flow domain measuring their quality.

5.1 Grid Independency Test

In finite element method, it is essential to determine the grid size considering sufficient number of elements in the resolution field to obtain a converged solution. In the present analysis we have done so considering CoFe₂O₄-EO nanofluid when $Pr = 6.84$, $Ra_T = 10^6$, $Ra_C = 10^4$, $\phi^* = 0.1$, $D^* = 0.5$, $H^* = 0.4$, $Ha = 10$, $\gamma = 30^\circ$, $n = 3$, $d_p = 10nm$ and $\tau = 10$. Grid independency is tested considering six dissimilar non-uniform grids such as coarse, normal, fine, finer, extra fine and extremely fine having 1024, 1537, 2527, 6518, 17036 and 26436 number of elements in the resolution field. Fig. 3 displays the rate of heat transfer(Nu_{ave}) against the number of elements for the above-said grid sizes. This figure shows that value of Nu_{ave} changes slightly for 17036 and 26436 elements. Thus, for the numerical simulation, 17036 elements for the grid independent solutions have been used.

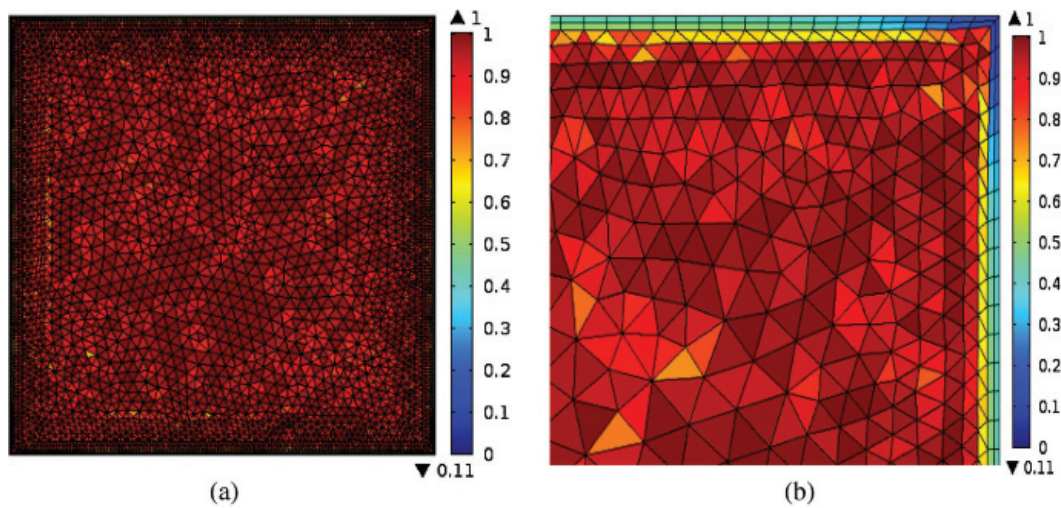


Figure 2: (a) Grid generation of the square-shape cavity with legend of quality measure, (b) the zoom in the upper right-corner of the cavity

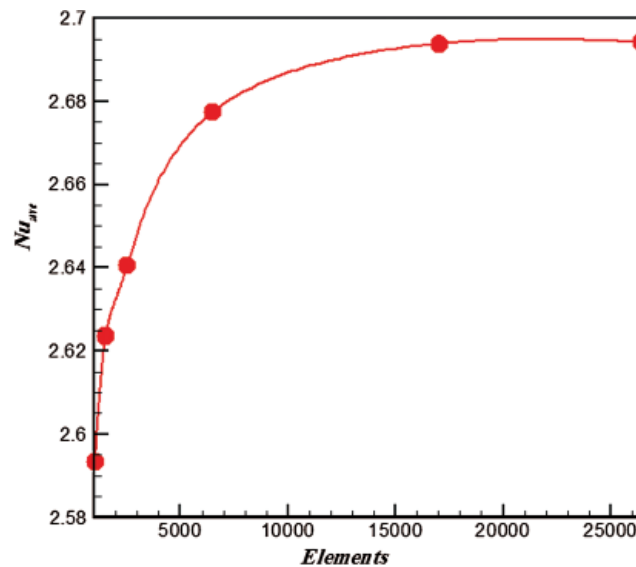


Figure 3: Grid independency test for CoFe₂O₄-EO nanofluid considering $Pr = 6.84$, $Ra_T = 10^6$, $Ra_C = 10^4$, $D^* = 0.5$, $\phi^* = 0.1$, $H^* = 0.4$, $Ha = 10$, $\gamma = 30^\circ$, $d_p = 10nm$, $n = 3$ and $\tau = 10$

5.2 Code Validity

The precision of the current code is checked for a base fluid with the outcomes of Nguyen et al. [2], Aminossadati et al. [18], and Cheikh et al. [47] when $Ra_T = 10^4$, $Pr = 6.83$, $D^* = 0.5$, $H^* = 0.2$, $Ha = 0$, $\gamma = 0^\circ$ and $\phi^* = 0$ in the absence of the concentration equation. The comparisons of the data displayed in Tab. 3 are quite appreciable.

6 Results and Discussion

The numerically simulated results are obtained for an unsteady 2D free convection flow of magnetic nanofluids in the presence of a sloped magnetic field inside a square cavity for different model parameters especially the thermal Rayleigh number $10^5 \leq Ra_T \leq 10^6$, nanoparticles solid volume fraction

Table 3: Comparison of the average Nusselt number (Nu_{ave}) with Nguyen et al. [2], Cheikh et al. [47] and Aminossadati et al. [18] when $\phi^* = 0$

H	$H = 0.2$				$H = 0.8$			
	$Ra_T = 10^3$		$Ra_T = 10^4$		$Ra_T = 10^3$		$Ra_T = 10^4$	
Ra_T	Nu_{ave}	θ_{max}	Nu_{ave}	θ_{max}	Nu_{ave}	θ_{max}	Nu_{ave}	θ_{max}
Published paper								
Nguyen et al. [2]	5.941	0.181	5.941	0.180	3.512	0.363	3.756	0.363
Cheikh et al. [47]	5.947	0.182	5.947	0.182	3.553	0.364	3.805	0.364
Aminossadati et al. [18]	5.954	0.182	5.954	0.182	3.555	0.364	3.806	0.364
Present study	5.944	0.182	5.954	0.181	3.550	0.362	3.751	0.364

$0 \leq \phi^* \leq 0.1$, the Hartmann number $0 \leq Ha \leq 40$, heat flux length $0.2 \leq H^* \leq 0.8$, and heat flux locations ($0.2 \leq D^* \leq 0.5$). Ferrite-water was considered nanofluid as default unless otherwise specified.

6.1 Effects of Thermal Rayleigh Number and Nanoparticles Loading

Fig. 4 displays the influences of increasing the nanoparticles loading (or volume fraction) (ϕ^*) and thermal buoyancy parameter on the streamlines for $Pr = 6.84$, $Ra_T = 10^6$, $Ra_C = 10^4$, $Ha = 10$,

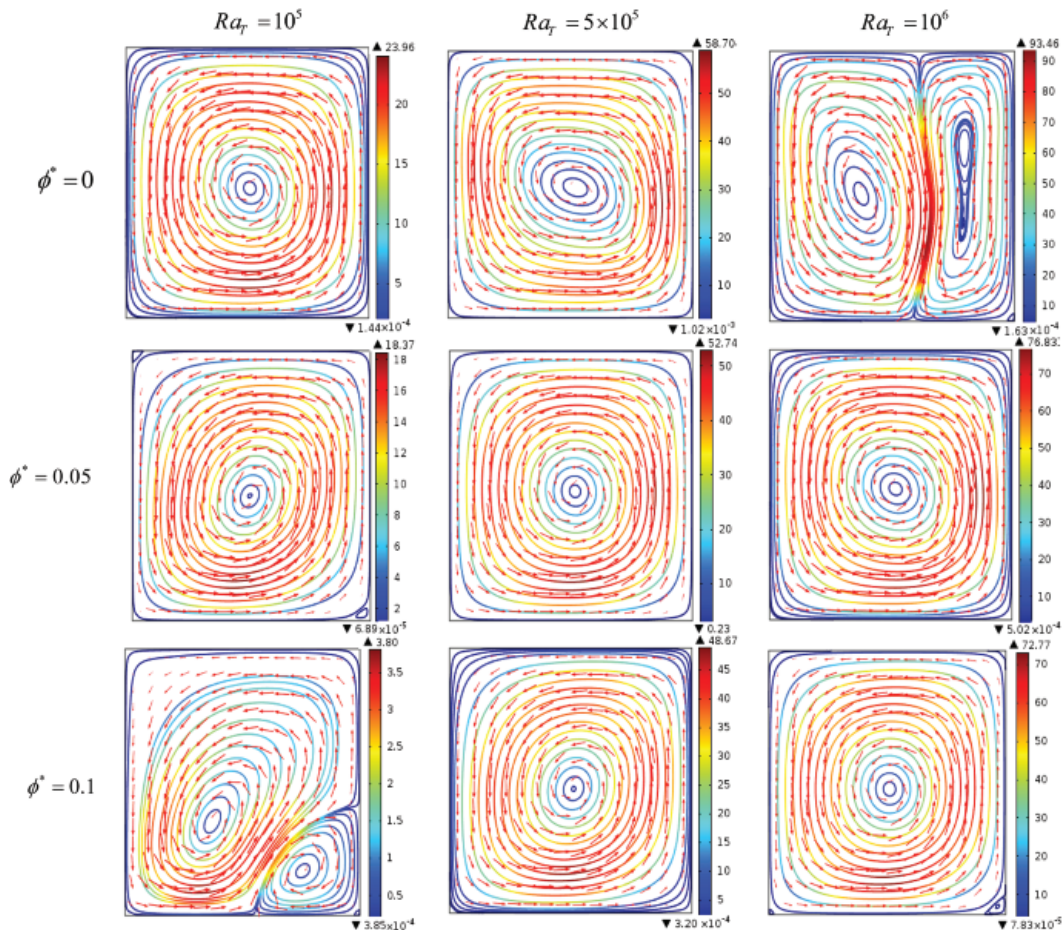


Figure 4: The streamlines for Fe_3O_4 - H_2O nanofluid at $\phi^* = 0, 0.05$ and 0.1 when $Pr = 6.84$, $Ra_T = 10^6$, $Ra_C = 10^4$, $Ha = 10$, $D^* = 0.5$, $H^* = 0.4$, $\gamma = 30^\circ$, $d_p = 10$ nm, $n = 3$ and $\tau = 10$

$D^* = 0.5, H^* = 0.4, \gamma = 30^\circ, d_p = 10 \text{ nm}, n = 3$ and $\tau = 10$. For a base fluid ($\phi^* = 0$) at $Ra_T = 10^5$ one anticlockwise rotating bigger vortex appears. As the buoyancy-driven parameter increases to $Ra_T = 10^6$, the bigger vortex divides into two vertically asymmetrical vortices with the opposite direction of motion. On the other hand when the solid volume fraction intensifies, an oppositely rotating smaller vortex appears at the lower right corner of the cavity for $Ra_T = 10^5$. The intensity of this smaller vortex increases with the further increase of the solid volume fraction of the nanofluid. Interestingly, when the thermal buoyancy parameter further increases to $Ra_T = 10^6$ the smaller vortex diminishes. For a fixed amount of nanoparticle loading, the intensity of the surface velocity intensifies when the thermal Rayleigh number increases. It reduces with the increase of the amount of nanoparticles loading for a fixed Rayleigh number. Thus, the thermal Rayleigh number and nanoparticle volume fraction, significantly control the nanofluid flow dynamics.

The evolutions of isotherms varying thermal Rayleigh number and nanoparticle concentration when $Pr = 6.84, Ra_T = 10^6, Ra_C = 10^4, Ha = 10, D^* = 0.5, H^* = 0.4, \gamma = 30^\circ, d_p = 10 \text{ nm}, n = 3$ and $\tau = 10$ are shown in Fig. 5. For a regular fluid ($\phi^* = 0$), the isotherm lines are distributed in the entire cavity and condensed near the heat flux. As buoyancy-driven parameter escalates, the isotherm lines are condensed and squeezed together near the heat flux wall of the enclosure especially at $Ra_T = 10^6$ which

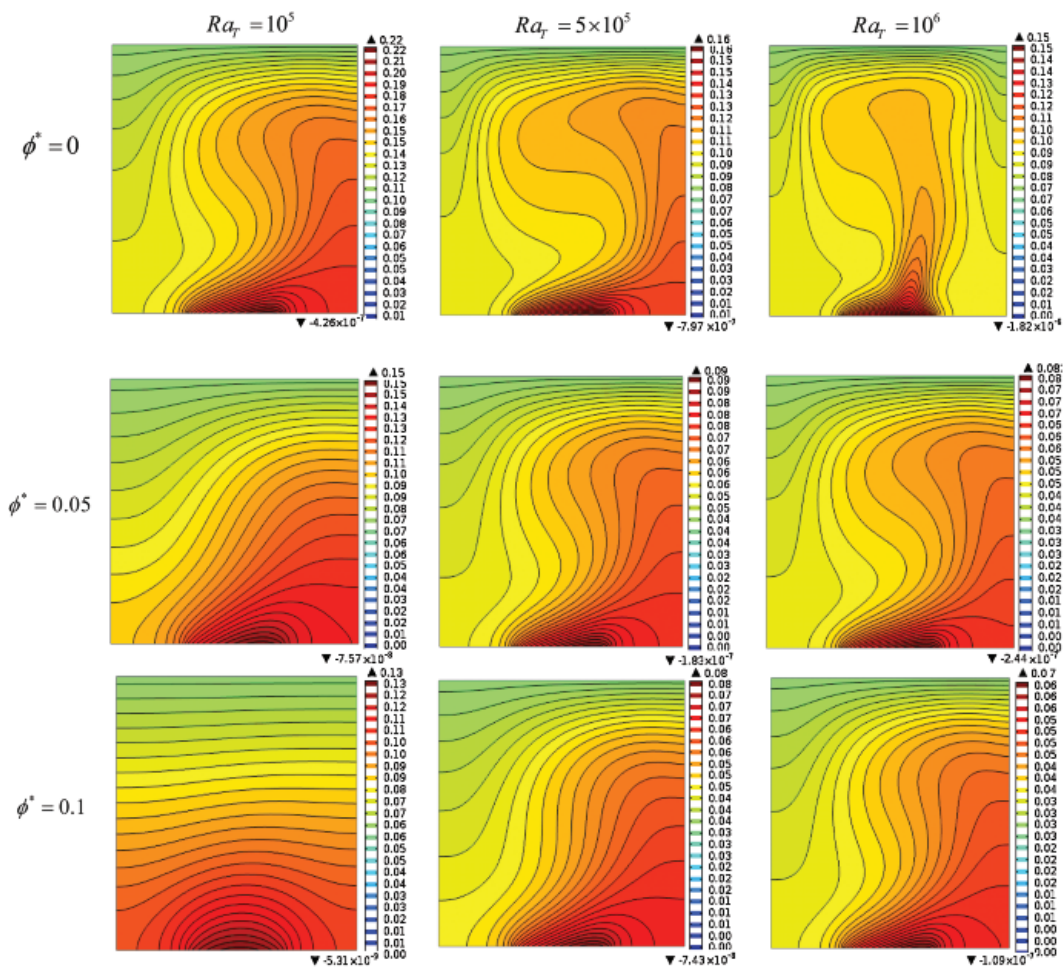


Figure 5: The isotherms for Fe₃O₄-H₂O nanofluid at $\phi = 0, 0.05, 0.1$ when $Pr = 6.84, Ra_T = 10^6, Ra_C = 10^4, Ha = 10, D^* = 0.5, H^* = 0.4, \gamma = 30^\circ, d_p = 10 \text{ nm}, n = 3$ and $\tau = 10$

is an indication of a high level of convection. Adding nanoparticles to a regular fluid reduces the temperature rate which is an indication of enhanced performance of cavity cooling. At $Ra_T = 10^5$, as nanoparticles volume fraction intensifies, the isotherm lines become parallel to each other and become parabolic in shape at heat flux which signposts that conduction is the dominant mode of heat transfer. The influences of varying Ra_T and ϕ^* on isoconcentrations loop when $Pr = 6.84$, $Ra_T = 10^6$, $Ra_C = 10^4$, $Ha = 10$, $D^* = 0.5$, $H^* = 0.4$, $\gamma = 30^\circ$, $n = 3$, $d_p = 10 \text{ nm}$ and $\tau = 10$ are exhibited in Fig. 6. Remarkably, the loops of isoconcentrations have similar behavior of streamlines but their appearances are skinny and feeble due to the advanced Brownian diffusion. Also, levels of isoconcentrations, as well as their loops, are distributed in the entire domain of the enclosure and condensed on the cooled and adiabatic wall where temperatures are low due to thermophoresis phenomenon which intensifies buoyancy-driven force and concentrations of nanoparticles.

6.2 The Effects of Sloped Magnetic Field

Effects of magnetic field (Ha) on the flow, thermal and concentration fields when $Pr = 6.84$, $Ra_T = 10^6$, $Ra_C = 10^4$, $H^* = 0.4$, $D^* = 0.5$, $\phi^* = 0.1$, $\gamma = 30^\circ$, $n = 3$, $d_p = 10 \text{ nm}$ and $\tau = 10$ are demonstrated in Fig. 7. For $Ha = 0$, i.e., in the absence of an applied magnetic field, the streamlines are divided into two symmetrical vortices with an opposite direction of motion. Furthermore, the isotherm lines are squeezed close to the heat flux taking a mushroom pattern with strong convection when $Ha = 0$. While Ha is

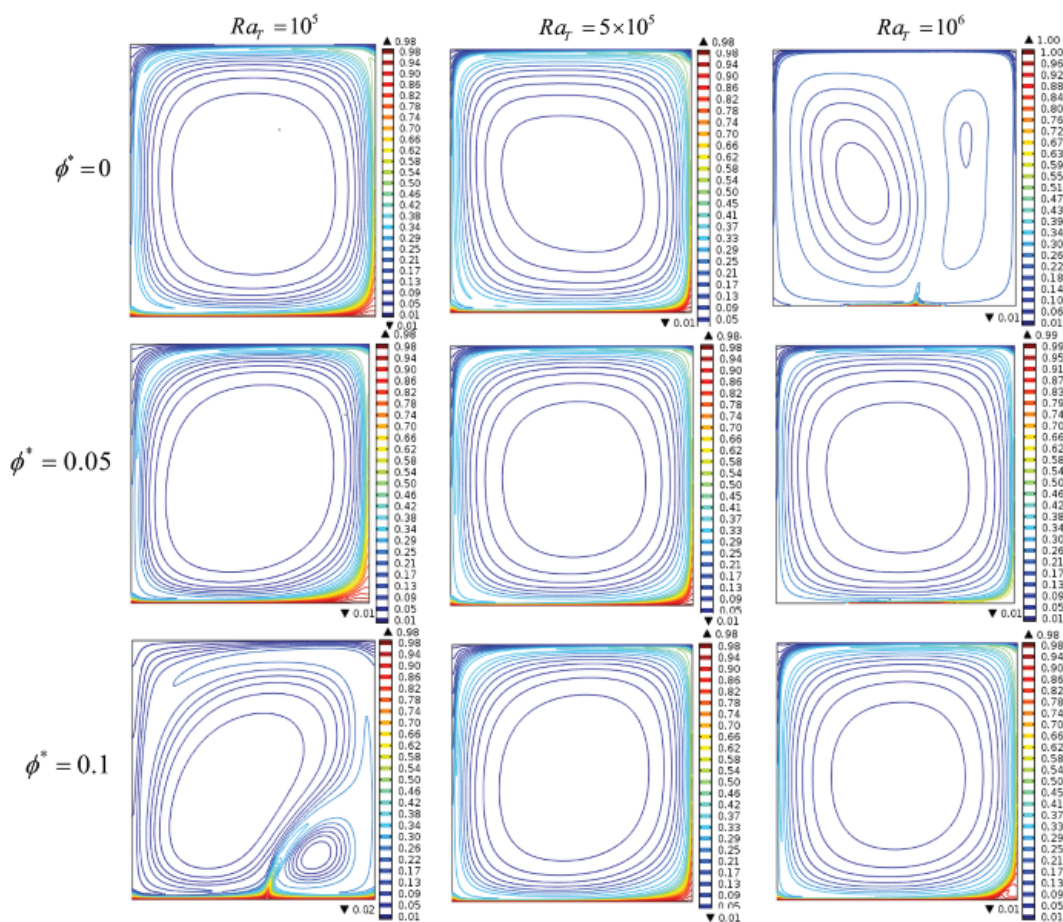


Figure 6: The isoconcentrations for $\text{Fe}_3\text{O}_4\text{-H}_2\text{O}$ nanofluid at $\phi = 0, 0.05$ and 0.1 when $Pr = 6.84$, $Ra_T = 10^6$, $Ra_C = 10^4$, $Ha = 10$, $D^* = 0.5$, $H^* = 0.4$, $\gamma = 30^\circ$, $d_p = 10 \text{ nm}$, $n = 3$ and $\tau = 10$

increased, the convection flow is affected by the magnetic field. The maximum surface velocity falls with the increase of Ha caused by the Lorentz force. Consequently, one bigger vortex rotates anticlockwise along with a small vortex that appears at the bottom right corner of the cavity. As Hartmann's number increases this small vortex becomes bigger and rotates clockwise. This also intensifies the strength and density of the streamlines.

Fig. 7 further reveals that a stronger magnetic field ($Ha \geq 30$) forced the isotherm lines to become almost parallel to each other and suppresses the convection currents. As expected, the isoconcentrations loops become lean and delicate because of the higher Brownian diffusion.

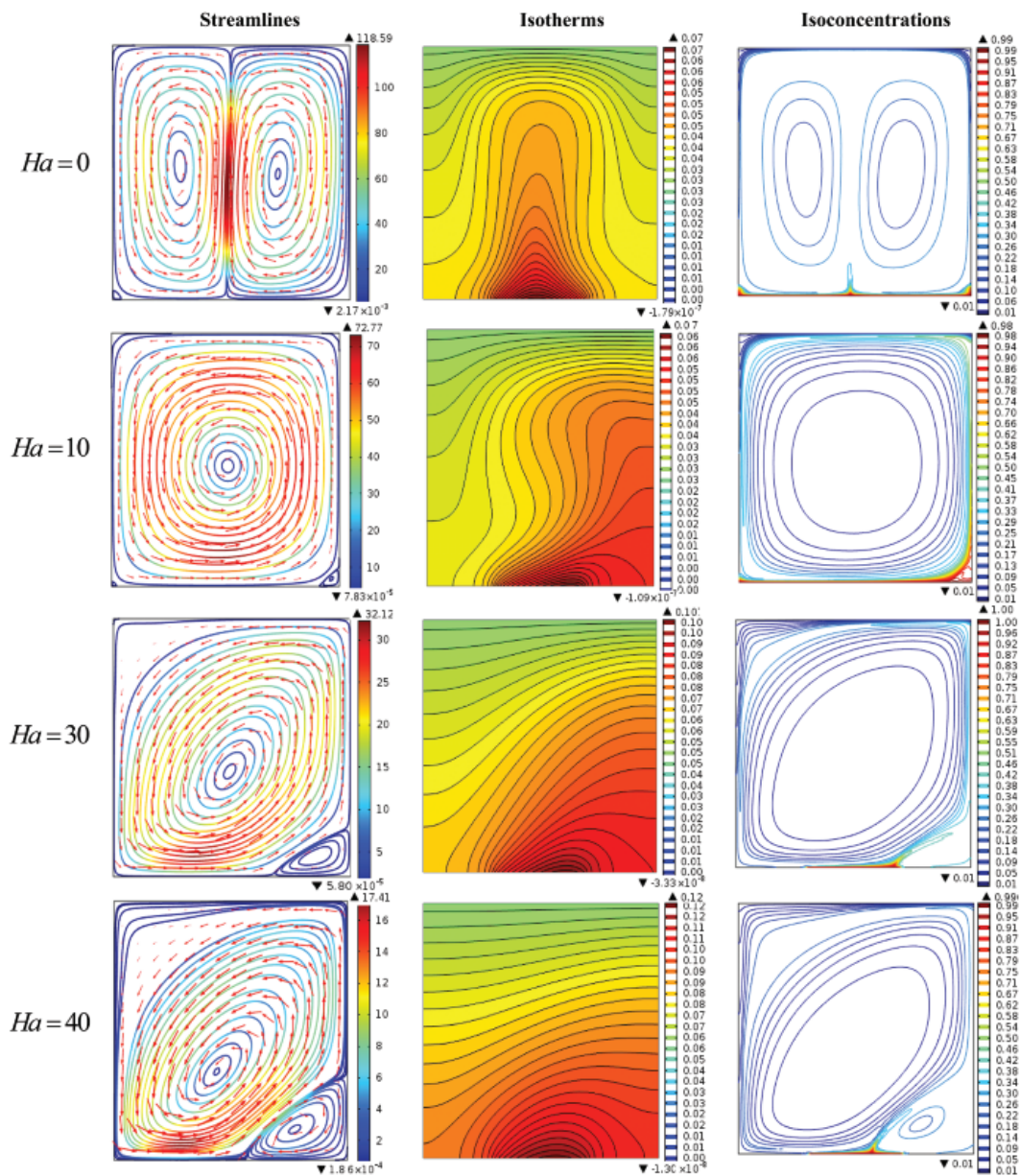


Figure 7: The streamlines, isotherms and isoconcentrations for $Fe_3O_4-H_2O$ at $Ha = 0, 10, 20, 30$ and 40 when $Pr = 6.84, Ra_T = 10^6, Ra_C = 10^4, H^* = 0.4, D^* = 0.5, \phi^* = 0.1, \gamma = 30^\circ, d_p = 10 \text{ nm}, n = 3$ and $\tau = 10$

6.3 The Effects of Heat Flux Length

The effects of heat flux length $H^* = 0.2, 0.4, 0.6$ and 0.8 on streamlines, isotherms and isoconcentrations of nanofluid when $Pr = 6.84, Ra_T = 10^6, Ra_C = 10^4, Ha = 10, D^* = 0.5, \phi^* = 0.1, \gamma = 30^\circ, d_p = 10 \text{ nm}, n = 3$ and $\tau = 10$ are depicted in Fig. 8.

As the heat flux length the fluid motion within the cavity also intensifies due to the enhancement of the buoyancy force. Additionally, there appears a stronger anticlockwise circulation in streamlines within the entire cavity when H^* strengthens. As the length of heat flux H^* upsurges, the generated amount of heat

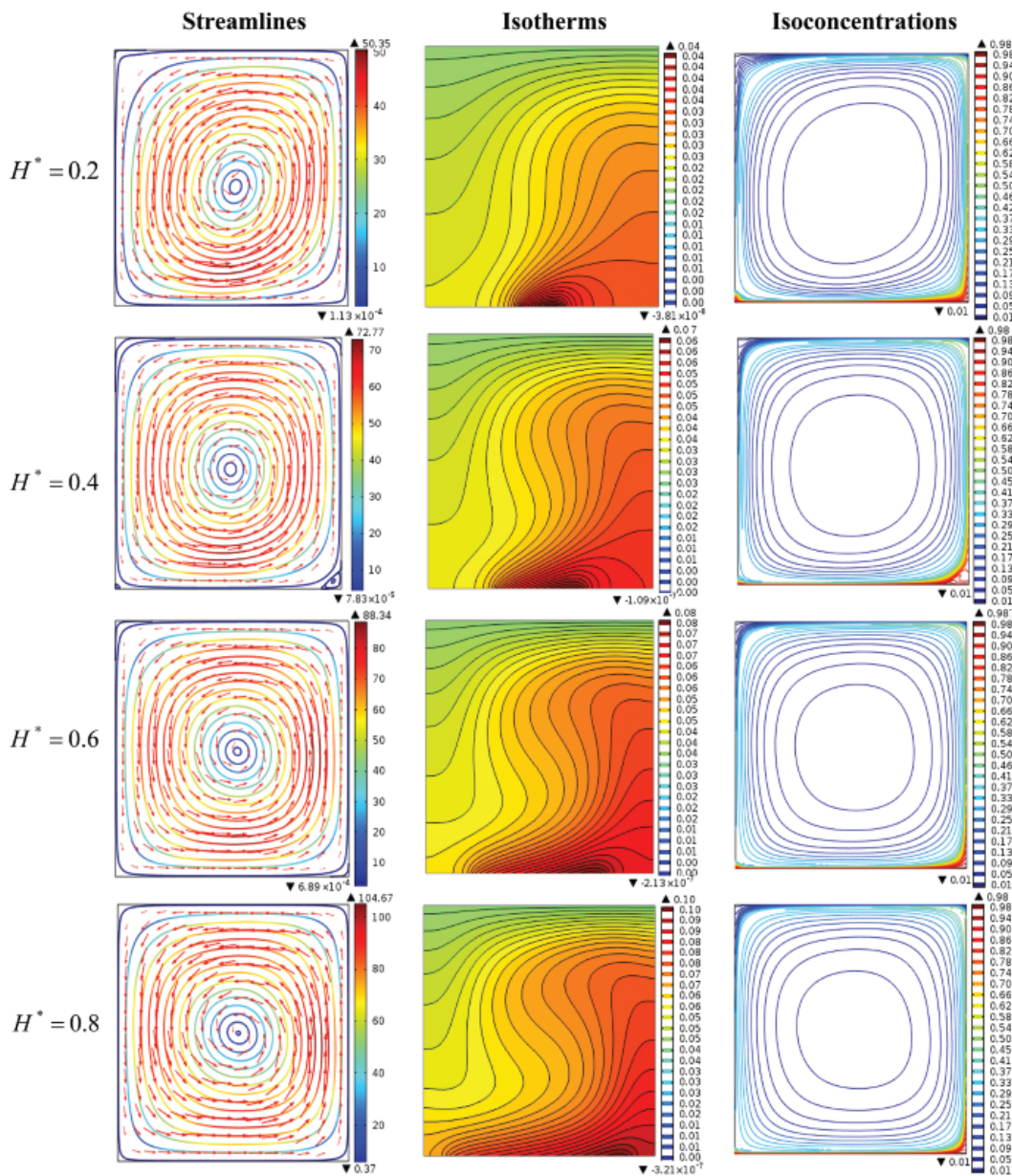


Figure 8: The streamlines, isotherms and isoconcentrations for $Fe_3O_4-H_2O$ at $H = 0.2, 0.4, 0.6$ and 0.8 when $Pr = 6.84, Ra_T = 10^6, Ra_C = 10^4, Ha = 10, D^* = 0.5, \phi^* = 0.1, \gamma = 30^\circ, d_p = 10 \text{ nm}, n = 3$ and $\tau = 10$

escalates the isotherms intensity. On the other hand, the isoconcentrations loops distributed in the entire enclosure become less condensed when heat source length increases.

6.4 The Effects of Heat Flux Location

The evolutions of streamlines, isotherms and isoconcentrations with different heat flux locations $D^* = 0.2, 0.3, 0.4$ and 0.5 are displayed in Fig. 9 when $Pr = 6.84, Ra_T = 10^6, Ra_C = 10^4, Ha = 10, H^* = 0.4, \phi^* = 0.1, \gamma = 30^\circ, d_p = 10 \text{ nm}, n = 3$ and $\tau = 10$. For streamlines, we detected a bigger vortex circulating clockwise whereas two small vortices located at the left (top) and the right (bottom) corners of

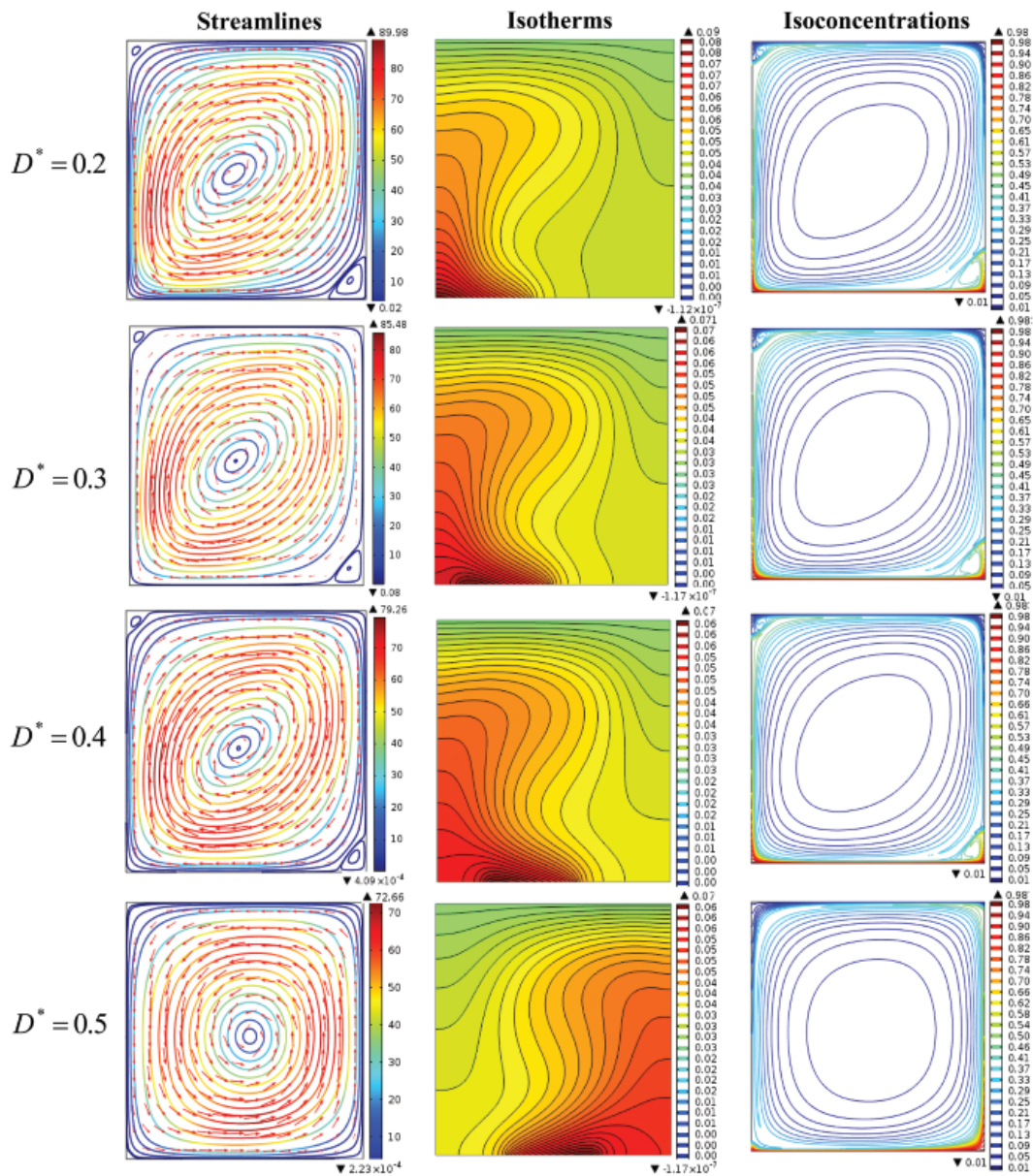


Figure 9: The streamlines, isotherms and isoconcentrations for $Fe_3O_4-H_2O$ nanofuid at $D^* = 0.2, 0.3, 0.4$ and 0.5 when $Pr = 6.84, Ra_T = 10^6, Ra_C = 10^4, Ha = 10, H^* = 0.4, \phi^* = 0.1, \gamma = 30^\circ, d_p = 10 \text{ nm}, n = 3$ and $\tau = 10$

the enclosure, circulating anticlockwise. The maximum surface velocity decreases as the heat flux shifts toward the center of the cavity. The isotherm lines are affected by varying the heat flux location. The temperature rate is decreased slowly as the heat source shifts toward the center of the cavity.

The effects of D^* on the isoconcentrations are also quite noticeable. As D^* increases, the inner shape of the isoconcentrations loops changes from oblate to almost circular and the small vortices appear at corners, top left and bottom right, vanish.

6.5 The Average Nusselt Number Varying Ha , H^* , D^* , ϕ^* and n

Fig. 10 exhibits the rate of heat transfer (Nu_{ave}) in Fe_3O_4 - H_2O nanofluid for different values of the Hartmann number Ha , heat flux length H^* , heat flux location D^* and particle shape n varying nanoparticles loading ϕ^* when $Pr = 6.84$, $Ra_T = 10^5$, $Ra_C = 10^3$, $d_p = 10$ and $\tau = 2$. Figs. 10a–10c illustrate that for a spherical shape nanoparticles, the Nu_{ave} declines with the escalation of Ha , H^* and D^* while it rises with the increase of ϕ^* . In Fig. 10d, we demonstrates the variation of average Nusselt number considering spherical, brick, cylindrical, platelet and blade shape Fe_3O_4 nanoparticles in water. This figure reveals that irrespective of the nanoparticles loading, the highest average Nusselt number is found for the blade shape nanoparticles and lowest for the spherical shape. It is significant that blade shape nanoparticles provide a 9.64% increase of the average Nusselt number as compared to the spherical shape.

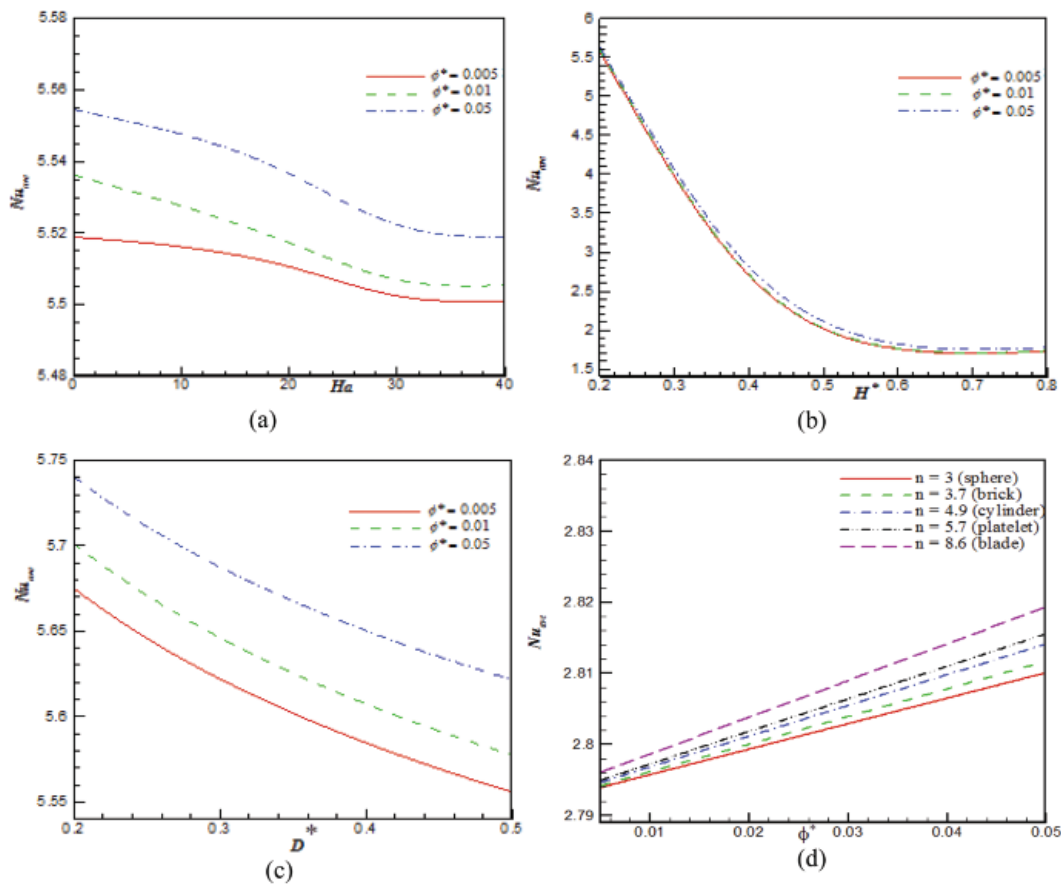


Figure 10: The average Nusselt number Nu_{ave} for Fe_3O_4 - H_2O for different (a) ϕ^* and Ha , (b) ϕ^* and H^* , (c) ϕ^* and D^* (d) ϕ^* and n when $Pr = 6.84$, $Ra_T = 10^5$, $Ra_C = 10^3$, $\gamma = 30^\circ$, $d_p = 10$ nm, and $\tau = 2$

6.6 The Average Nusselt Number for Different Nanofluids

The average Nusselt numbers for 12 types of nanofluids considering water (H₂O), kerosene (Ke) and engine oil (EO) as regular fluids utilizing magnetic nanoparticles called ferrite (Fe₃O₄), Mn-Zn ferrite (Mn-ZnFe₂O₄), cobalt ferrite (CoFe₂O₄) and silicon dioxide (SiO₂) are depicted in Fig. 11. From the comparative analysis, we found that kerosene-based nanofluids provide the highest rate of heat transfer. Mn-Zn ferrite offers highest increase, 3.62% of the average Nusselt number compared to the SiO₂ nanoparticles which provide the lowest rate of heat transfer among magnetic nanoparticles having kerosene as base fluid at nanoparticles concentration level $\phi^* = 0.05$.

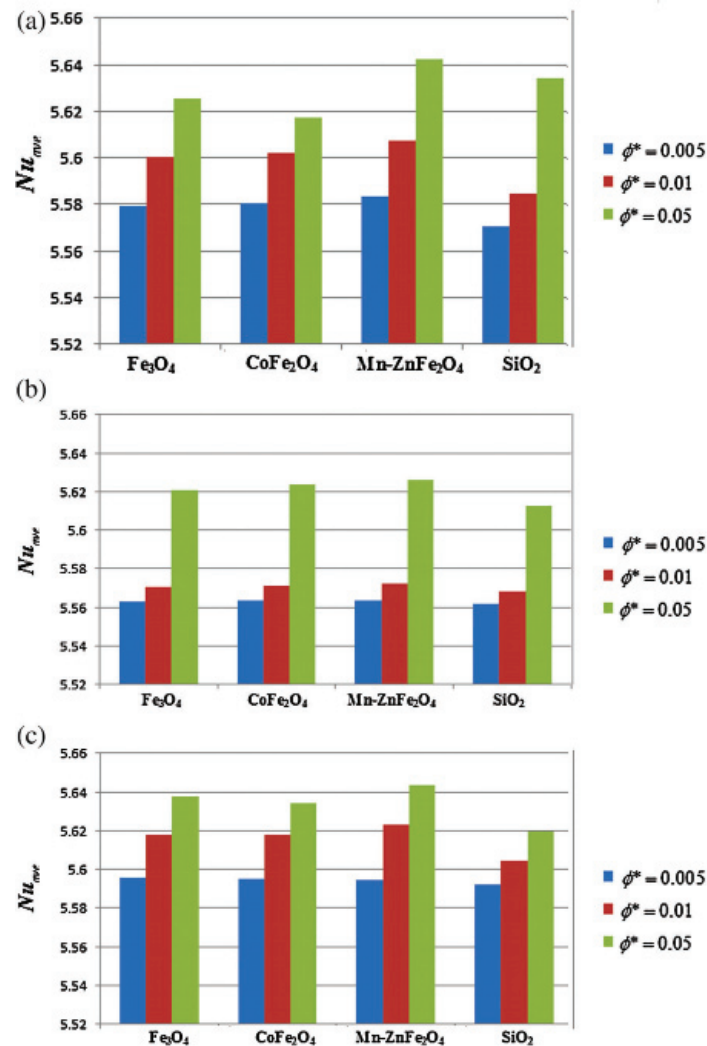


Figure 11: The average Nusselt number for (a) water, (b) engine oil, (c) kerosene with different nanoparticles when $Pr = 6.84$, $Ra_T = 10^5$, $Ra_C = 10^3$, $Ha = 10$, $D^* = 0.5$, $H^* = 0.2$, $\gamma = 30^\circ$, $d_p = 10\text{ nm}$, $n = 3$ and $\tau = 2$

7 Conclusions

The unsteady buoyancy-driven heat transfer flow, in a square cavity energized by the heat flux at the bottom of the lower edge of the cavity, using a nonhomogeneous dynamic model under the influence of a sloping magnetic field, utilizing magnetic nanoparticles, has been simulated numerically. Comparisons are

made between current outcomes with the earlier published data and very good agreement is achieved. Influences of numerous model parameters especially the thermal Rayleigh number, the Hartmann number, the heat flux length, the heat flux location, the solid volume fraction and nanoparticles shape on the flow, thermal and concentration fields have been studied numerically. Our simulations have led the following major conclusions:

- The flow, thermal and concentration fields are modified remarkably with the increase of the thermal Rayleigh number, Hartmann number, heat flux length and position, and the nanoparticle loading.
- The heat transfer rate Nu_{ave} decreases with the increase of Ha , H^* , D^* and ϕ^* .
- Kerosene based nanofluids noticeably provide the highest rate of heat transfer, a 4.33% increase compared to the engine oil which provides the lowest rate.
- Mn-Zn ferrite-Ke shows the highest heat transfer rate among magnetic nanofluids. It gives a 3.62% increase compared to the SiO₂-Ke; which provides the lowest heat transfer rate.
- Blade, platelet, cylinder and brick shape nanoparticles provides almost 10%, 5.8%, 3.9%, and 1.6%, respectively, an increase in the average Nusselt number compared to the spherical shape.

Acknowledgement: The authors would like to thank the anonymous referees for their valuable comments for the further improvement of the paper.

Funding Statement: This work was supported by the Sultan Qaboos University [IG/SCI/DOMS/18/10].

Conflicts of Interest: The authors declare that they have no conflicts of interest to report regarding the present study.

References

1. Choi, S. U. S. (1995). Enhancing thermal conductivity of fluids with nanoparticles. *International Mechanical Engineering Congress & Exposition*, 66, 99–105.
2. Nguyen, M. T., Aly, A. M., Lee, S. W. (2016). Unsteady natural convection heat transfer in a nanofluid-filled square cavity with various heat source conditions. *Advances in Mechanical Engineering*, 8(5), 10.1177/1687814016646547.
3. Mansour, M. A., Ahmed, S. E. (2012). Mixed convection flows in a square lid-driven cavity with heat source at the bottom utilizing nanofluid. *Canadian Journal of Chemical Engineering*, 90(1), 100–110. DOI 10.1002/cjce.20533.
4. Öztop, H. F., Sakhrieh, A., Abu-Nada, E., Al-Salem, K. (2017). Mixed convection of MHD flow in nanofluid filled and partially heated wavy walled lid-driven enclosure. *International Communications in Heat & Mass*, 86, 42–51. DOI 10.1016/j.icheatmasstransfer.2017.05.011.
5. Hemmat Esfe, M., Saedodin, S., Hasani Malekshah, E., Babaie, A., Rostamian, H. (2019). Mixed convection inside lid-driven cavities filled with nanofluids. *Journal of Thermal Analysis and Calorimetry*, 135(1), 813–859. DOI 10.1007/s10973-018-7519-x.
6. Bondarenko, D. S., Sheremet, M. A., Oztop, H. F., Abu-Hamdeh, N. (2019). Mixed convection heat transfer of a nanofluid in a lid-driven enclosure with two adherent porous blocks. *Journal of Thermal Analysis and Calorimetry*, 135(2), 1095–1105. DOI 10.1007/s10973-018-7455-9.
7. Astanina, M. S., Riahi, M. K., Abu-Nada, E., Sheremet, M. A. (2018). Magnetohydrodynamic in partially heated square cavity with variable properties: discrepancy in experimental and theoretical conductivity correlations. *International Journal of Heat and Mass Transfer*, 116, 532–548. DOI 10.1016/j.ijheatmasstransfer.2017.09.050.
8. Park, J., Kim, M., Mun, G. S., Park, Y. G., Ha, M. Y. (2018). Natural convection in a square enclosure with a circular cylinder with adiabatic side walls according to bottom wall temperature variation. *Journal of Mechanical Science and Technology*, 32(7), 3201–3211. DOI 10.1007/s12206-018-0623-9.
9. Jahanbakhshi, A., Nadooshan, A. A., Bayareh, M. (2018). Magnetic field effects on natural convection flow of a non-Newtonian fluid in an L-shaped enclosure. *Journal of Thermal Analysis and Calorimetry*, 133(3), 1407–1416. DOI 10.1007/s10973-018-7219-6.

10. Sheremet, M. A., Pop, I., Mahian, O. (2018). Natural convection in an inclined cavity with time-periodic temperature boundary conditions using nanofluids: application in solar collectors. *International Journal of Heat and Mass Transfer*, 116, 751–761. DOI 10.1016/j.ijheatmasstransfer.2017.09.070.
11. Cho, H. W., Park, Y. G., Ha, M. Y. (2018). The natural convection in a square enclosure with two hot inner cylinders, part I: the effect of one elliptical cylinder with various aspect ratios in a vertical array. *International Journal of Heat and Mass Transfer*, 125, 815–827. DOI 10.1016/j.ijheatmasstransfer.2018.04.141.
12. Sheikhzadeh, G. A., Aghaei, A. (2018). Effect of nanoparticle shape on natural convection heat transfer in a square cavity with partitions using water-SiO₂ nanofluid. *Transport Phenomena in Nano and Micro Scales*, 6(1), 27–38.
13. Shahriari, A., Javaran, E. J., Rahnama, M. (2018). Effect of nanoparticles Brownian motion and uniform sinusoidal roughness elements on natural convection in an enclosure. *Journal of Thermal Analysis and Calorimetry*, 131(3), 2865–2884. DOI 10.1007/s10973-017-6787-1.
14. Mehryan, S. A. M., Ghalambaz, M., Izadi, M. (2019). Conjugate natural convection of nanofluids inside an enclosure filled by three layers of solid, porous medium and free nanofluid using Buongiorno's and local thermal non-equilibrium models. *Journal of Thermal Analysis and Calorimetry*, 135(2), 1047–1067. DOI 10.1007/s10973-018-7380-y.
15. Alsabery, A. I., Ishak, M. S., Chamkha, A. J., Hashim, I. (2018). Entropy generation analysis and natural convection in a nanofluid-filled square cavity with a concentric solid insert and different temperature distributions. *Entropy*, 20(336), 336. DOI 10.3390/e20050336.
16. Alsabery, A., Tayebi, T., Chamkha, A., Hashim, I. (2018). Effects of non-homogeneous nanofluid model on natural convection in a square cavity in the presence of conducting solid block and corner heater. *Energies*, 11(2507), 2507. DOI 10.3390/en11102507.
17. Sezai, I., Mohamad, A. A. (2000). Natural convection from a discrete heat source on the bottom of a horizontal enclosure. *International Journal of Heat and Mass Transfer*, 43(13), 2257–2266. DOI 10.1016/S0017-9310(99)00304-X.
18. Aminossadati, S. M., Ghasemi, B. (2009). Natural convection cooling of a localized heat source at the bottom of a nanofluid-filled enclosure. *European Journal of Mechanics B/Fluids*, 28(5), 630–640. DOI 10.1016/j.euromechflu.2009.05.006.
19. Saravanan, S., Hakeem, A. A., Kandaswamy, P. K. (2009). Natural convection in a cavity with orthogonal heat-generating baffles of different lengths. *Heat Transfer Research*, 40(8), 805–819. DOI 10.1615/HeatTransRes.v40.i8.60.
20. Kandaswamy, P., Lee, J., Hakeem, A. A., Saravanan, S. (2008). Effect of baffle—cavity ratios on buoyancy convection in a cavity with mutually orthogonal heated baffles. *International Journal of Heat and Mass Transfer*, 51(7–8), 1830–1837. DOI 10.1016/j.ijheatmasstransfer.2007.06.039.
21. Saravanan, S., Hakeem, A. A., Kandaswamy, P., Lee, J. (2008). Buoyancy convection in a cavity with mutually orthogonal heated plates. *Computers & Mathematics with Applications*, 55(12), 2903–2912. DOI 10.1016/j.camwa.2007.11.024.
22. Hakeem, A. A., Saravanan, S., Kandaswamy, P. (2008). Buoyancy convection in a square cavity with mutually orthogonal heat generating baffles. *International Journal of Heat and Fluid Flow*, 29(4), 1164–1173. DOI 10.1016/j.ijheatfluidflow.2008.01.015.
23. Alsabery, A. I., Sheremet, M. A., Chamkha, A. J., Hashim, I. (2018). Conjugate natural convection of Al₂O₃—water nanofluid in a square cavity with a concentric solid insert using Buongiorno's two-phase model. *International Journal of Mechanical Science*, 136, 200–219. DOI 10.1016/j.ijmecsci.2017.12.025.
24. Alsabery, A. I., Ismael, M. A., Chamkha, A. J., Hashim, I. (2019). Effects of two-phase nanofluid model on MHD mixed convection in a lid-driven cavity in the presence of conductive inner block and corner heater. *Journal of Thermal Analysis and Calorimetry*, 135(1), 729–750. DOI 10.1007/s10973-018-7377-6.
25. Al Kalbani, K. S., Rahman, M. M. (2019). Investigation of the local thermal nonequilibrium conditions for a convective heat transfer flow in an inclined square enclosure filled with Cu-water nanofluid. *Arabian Journal for Science and Engineering*, 44(2), 1337–1351. DOI 10.1007/s13369-018-3514-6.

26. Uddin, M. J., Rahman, M. M., Alam, M. S. (2018). Analysis of natural convective heat transport in homocentric annuli containing nanofluids with an oriented magnetic field using nonhomogeneous dynamic model. *Neural Computing and Applications*, 30(10), 3189–3208. DOI 10.1007/s00521-017-2905-z.
27. Uddin, M. J., Fazlul Hoque, A. K. M., Rahman, M. M., Vajravelu, K. (2019). Numerical simulation of convective heat transport within the nanofluid filled vertical tube of plain and uneven side walls. *International Journal of Thermofluid Science and Technology*, 6(1), 19060101. DOI 10.36963/IJTST.
28. Uddin, M. J., Rahman, M. M. (2018). Finite element computational procedure for convective flow of nanofluids in an annulus. *Thermal Science and Engineering Progress*, 6, 251–267. DOI 10.1016/j.tsep.2018.04.011.
29. Astanina, M. S., Sheremet, M. A. (2019). Simulation of mixed convection of a variable viscosity fluid in a partially porous horizontal channel with a heat-generating source. *Computer Research and Modeling*, 11(1), 95–107. DOI 10.20537/2076-7633-2019-11-1-95-107.
30. Sathiyamoorthy, M., Chamkha, A. (2010). Effect of magnetic field on natural convection flow in a liquid gallium filled square cavity for linearly heated side wall (s). *International Journal of Thermal Sciences*, 49(9), 1856–1865. DOI 10.1016/j.ijthermalsci.2010.04.014.
31. Mehryan, S. A. M., Sheremet, M. A., Soltani, M., Izadi, M. (2019). Natural convection of magnetic hybrid nanofluid inside a double-porous medium using two-equation energy model. *Journal of Molecular Liquids*, 277, 959–970. DOI 10.1016/j.molliq.2018.12.147.
32. Rahman, M. M., Pop, I., Saghir, M. Z. (2019). Steady free convection flow within a tilted nanofluid saturated porous cavity in the presence of a sloping magnetic field energized by an exothermic chemical reaction administered by Arrhenius kinetics. *International Journal of Heat and Mass Transfer*, 129, 198–211. DOI 10.1016/j.ijheatmasstransfer.2018.09.105.
33. Tiwari, R. J., Das, M. K. (2007). Heat transfer augmentation in a two-sided lid-driven differentially heated square cavity utilizing nanofluids. *International Journal of Heat and Mass Transfer*, 50(9–10), 2002–2018. DOI 10.1016/j.ijheatmasstransfer.2006.09.034.
34. Buongiorno, J. (2006). Convective transport in nanofluids. *Journal of Heat Transfer*, 128(3), 240–250. DOI 10.1115/1.2150834.
35. Uddin, M. J., Alam, M. S., Rahman, M. M. (2017). Natural convective heat transfer flow of nanofluids inside a quarter-circular enclosure using nonhomogeneous dynamic model. *Arabian Journal for Science and Engineering*, 42(5), 1883–1901. DOI 10.1007/s13369-016-2330-0.
36. Al Balushi, L. M., Uddin, M. J., Rahman, M. M. (2019). Natural convective heat transfer in a square enclosure utilizing magnetic nanoparticles. *Propulsion and Power Research*, 8(3), 194–209. DOI 10.1016/j.jprr.2018.07.009.
37. Al-Balushi, L. M., Rahman, M. M. (2019). Natural convective heat transfer in the presence of a sloping magnetic field inside a square enclosure with different wall temperature distributions utilizing magnetic nanoparticles following nonhomogeneous dynamic model. *Journal of Thermal Science and Engineering Applications*, 11(4), 041013.
38. Uddin, M. J., Rahman, M. M. (2017). Numerical computation of natural convective heat transport within nanofluids filled semi-circular shaped enclosure using nonhomogeneous dynamic model. *Thermal Science and Engineering Progress*, 1, 25–38. DOI 10.1016/j.tsep.2017.02.001.
39. Hafezisefat, P., Esfahany, M. N., Jafari, M. (2017). An experimental and numerical study of heat transfer in jacketed vessels by SiO₂ nanofluid. *Heat and Mass Transfer*, 53(7), 2395–2405. DOI 10.1007/s00231-017-1989-4.
40. Khan, W. A., Khan, Z. H., Haq, R. U. (2015). Flow and heat transfer of ferrofluids over a flat plate with uniform heat flux. *European Physical Journal Plus*, 130(86), 180. DOI 10.1140/epjp/i2015-15086-4.
41. Zienkiewicz, O. C., Taylor, R. L. (1991). *The finite element method*. 4th. edition, New York: McGraw-Hill.
42. Zienkiewicz, O. C., Taylor, R. L., Nithiarasu, P. (2014). *The finite element method for fluid dynamics*. 7th. edition, Oxford: Butterworth-Heinemann.

43. Codina, R. (1998). Comparison of some finite element methods for solving the diffusion-convection-reaction equation. *Computer Methods in Applied Mechanics and Engineering*, 156(1–4), 185–210. DOI 10.1016/S0045-7825(97)00206-5.
44. Uddin, M. J. (2017). *Flow dynamics of nanofluids inside a circular enclosure. (Ph.D. Thesis)*. SQU, Oman: College of Science.
45. Rahman, M. M., Alim, M. A., Mamun, M. A. H. (2009). Finite element analysis of mixed convection in a rectangular cavity with a heat-conducting horizontal circular cylinder. *Nonlinear Analysis: Modelling and Control*, 14(2), 217–247. DOI 10.15388/NA.2009.14.2.14522.
46. Al Kalbani, K. S., Alam, M. S., Rahman, M. M. (2016). Finite element analysis of unsteady natural convective heat transfer and fluid flow of nanofluids inside a tilted square enclosure in the presence of oriented magnetic field. *American Journal of Heat and Mass Transfer*, 3(3), 186–224.
47. Cheikh, N. B., Beya, B. B., Lili, T. (2007). Influence of the thermal boundary conditions on natural convection in a square enclosure partially heated from below. *International Communications in Heat and Mass Transfer*, 34(3), 369–379. DOI 10.1016/j.icheatmasstransfer.2006.11.001.